

# Strain-dependent fractional molecular diffusion in humid spider silk fibers

Igor Krasnov<sup>1,2</sup>, Tilo Seydel<sup>\*3</sup>, Imke Greving<sup>2</sup>, Malte Blankenburg<sup>1,2</sup>, Fritz Vollrath<sup>4</sup>, and Martin Müller<sup>1,2</sup>

<sup>1</sup>Institut für Experimentelle und Angewandte Physik, Universität Kiel, D-24098 Kiel, Germany

<sup>2</sup>Institute of Materials Research, Helmholtz-Zentrum Geesthacht (HZG), D-21502 Geesthacht, Germany

<sup>3</sup>Institut Max von Laue - Paul Langevin (ILL), CS 20156, F-38042 Grenoble, France

<sup>4</sup>Department of Zoology, University of Oxford, Oxford OX13PS, United Kingdom

August 25, 2016

## Abstract

Spider silk is a material well known for its outstanding mechanical properties, combining elasticity and tensile strength. The molecular mobility within the silk's polymer structure on the nanometer length scale importantly contributes to these macroscopic properties. We have therefore investigated the ensemble-averaged single-particle self-dynamics of the prevailing hydrogen atoms in humid spider dragline silk fibers on picosecond time scales *in situ* as a function of an externally applied tensile strain. We find that the molecular diffusion in the amorphous fraction of the oriented fibers can be described by a generalized fractional diffusion coefficient  $K_\alpha$  that is independent of the observation length scale in the probed range from approximately 0.3 to 3.5 nanometers.  $K_\alpha$  increases towards a diffusion coefficient of the classical Fickian type with increasing tensile strain consistent with an increasing loss of memory or entropy in the polymer matrix.

**Keywords:** spider dragline silk, fractional dynamics, nanocomposite polymer fibers, supercontraction, hydrophobic collapse, neutron spectroscopy

---

<sup>\*</sup>seydel@ill.eu

# 1 Introduction

Silk belongs to a large class of polymer nanocomposite materials currently of great fundamental and technological interest [1, 2, 3]. In particular, spider silk constitutes a remarkable elastomeric protein polymer fiber [4, 5]. An important fundamental question concerns the link between the mechanical properties of silk fibers and their origin on the level of molecular structure and dynamics [6, 7, 8], which has also been addressed by multiscale theory approaches [9, 10]. The molecular and mesoscopic structure of spider silk fibers has been explored rather comprehensively in the past (see e.g. [11, 12, 13, 14, 15, 16] and references therein) and been found to be consistent with a hierarchical structure of nanocrystallites interconnected within so-called nanofibrils by polymer regions with smectic order and being embedded in a disordered polymer matrix. The latter non-crystalline disordered polymer matrix is commonly denoted amorphous matrix [6].

The molecular dynamics aspects of the properties of silk associated with this hierarchical structure are subject to more recent attention. Whilst the nanocrystalline fraction of the fibers exclusively undergoes vibrational motions on the picosecond time scales relevant for molecular mobility [7], diffusive relaxation mechanisms on the molecular level can be associated with the amorphous fraction of the silk [14, 17, 18]. Importantly, water molecules may be inserted as tracer particles that selectively only access these amorphous regions [14, 7]. This technique allows detailed studies of the diffusive mobility of the hydrogen atoms of adsorbed water and the polymers themselves within the amorphous regions of silkworm silk fibers both as a function of humidity as well as as a function of an externally applied tensile stress [7, 17, 18]. It emerged that, in the complete absence of water, no diffusive but only vibrational mobility can be detected on picosecond time scales and nanometer length scales, and that includes the amorphous regions [7]. When water is adsorbed by the amorphous regions, both this water and the water-containing polymer matrix are subject to picosecond diffusive relaxations [17]. These diffusive relaxations can be interpreted in a “classical” picture of a superposition of diffusive dynamics in a geometrical confinement on molecular length scales [7]. When the silk fibers are exposed to a tensile strain, the geometry of this molecular confinement changes, which is reflected in the change of the associated diffusive molecular mobility [17]. However, the geometrical picture of a molecular confinement is limited by the highly heterogeneous disordered structure of the water-containing amorphous polymers.

Therefore, a more general model has been employed which quantitatively characterizes the observed dynamics whilst drastically reducing the number of free parameters. In this way, the molecular diffusive relaxation mechanisms in humid silkworm silk fibers have been found to be consistent with a picture of fractional Brownian dynamics [18]. In this picture, a generalized fractional diffusion coefficient

$$K_\alpha = \frac{\sigma_c^2}{\tau_c^\alpha} \quad (1)$$

describes the experimentally observed molecular diffusive processes of the amorphous polymer matrix entirely. Therein,  $\sigma_c$  and  $\tau_c$  are the characteristic spatial and time scales,

respectively, and the scalar  $0 < \alpha \leq 1$  is interpreted as the memory parameter of the system. For  $\alpha = 1$ , the diffusion would be of the classical Fickian type.  $K_\alpha$  is defined via the generalized fractional diffusion equation

$${}^C D^\alpha W(r, t) = K_\alpha \nabla^2 W(r, t), \quad (2)$$

where  $W(r, t)$  is the van Hove autocorrelation function depending on the particle coordinate  $r$  and time  $t$  and

$${}^C D^\alpha [\Phi](t) = \frac{1}{\Gamma(1 - \alpha)} \int_0^t \frac{\Phi'(\xi)}{(t - \xi)^\alpha} d\xi \quad (3)$$

is the operator defining the generalized fractional derivative of the function  $\Phi = \Phi(t)$ . Therein,  $\Phi'$  denotes the first-order integer derivative of  $\Phi$  and  $\Gamma(x)$  is the gamma function. The model of fractional diffusion is based on the assumption of a “waiting time” probability distribution with very long tails of particles undergoing “random walks” [19]. This picture describes the strongly confined diffusive atomic motions in polymeric materials. It is formulated by the generalized diffusion equation 2, which is solved by a generalized exponential function known as the Mittag-Leffler function. Moreover, it has been found that the same fractional calculus that provides the basis for the fractional molecular diffusion also describes the macroscopic mechanical properties of silkworm silk fibers [18], thus providing a link between molecular dynamical properties and the macroscopic mechanical behavior inspired by fractal concepts [20]. However, a comprehensive study of the function  $K_\alpha = K_\alpha(\sigma)$  relating the generalized fractional molecular diffusion coefficient to the applied strain  $\sigma$  on the fibers is still missing.

Spider silk fibers, although morphologically very similar to silkworm silk fibers [21], display a significantly higher amorphous fraction compared to the latter family of fibers. Humid spider dragline silk fibers also differ distinctly from humid silkworm silk fibers by showing supercontraction which is not shown by silkworm silk [22]. Supercontraction is induced when spider dragline silk is exposed to sufficiently high amounts of water for instance through high levels of ambient humidity above approximately 70 % [23, 24] and is associated with a drastic change of the morphological and mechanical properties. These morphological and mechanical differences as well as the overall superior mechanical properties underline the value of a detailed systematic investigation of the molecular diffusive dynamics in humid spider dragline silk fibers as a function of the tensile deformation of the fibers. Moreover, the supercontraction phenomenon may be understood in terms of a hydrophobic collapse of unfolded proteins [25, 26] related to similar observations made for elastin fibers [27].

Here we report the experimentally observed ensemble-averaged single-particle self-dynamics of the hydrogen atoms in humid spider dragline silk fibers on picosecond time scales and nanometer length scales as a function of an *in situ* applied tensile strain. We experimentally access the molecular self-dynamics unambiguously via the van Hove function  $W(r, t)$  using incoherent neutron scattering and we interpret and discuss the experimental results in terms of the established model of fractional Brownian diffusion,

equation 2. We associate the strain-dependent change in the observed molecular diffusion with the strain-dependent morphological changes in the fibers. It is worth noting that the required size of the spider dragline silk sample for a neutron spectroscopy experiment on the order of 100 mg constitutes an experimental challenge in itself. In passing, we also report the experimentally observed low-energy vibrational excitations of the prevailing hydrogen protons in our sample, which are obtained free from any selection rules using incoherent neutron scattering.

This article is organized as follows: In the subsequent sections, we present the neutron scattering experiment and data analysis procedures, followed by sections presenting the *in situ* recorded stress-strain curve of the humid spider silk sample as well as the equally *in situ* recorded neutron diffraction patterns and generalized frequency distributions obtained from the low-energy inelastic scattering. These sections serve to prepare the ground and establish the consistency of the essential results presented and discussed in the section on the quasi-elastic neutron scattering (QENS), immediately followed by our conclusions.

## 2 Experiment

We have used incoherent cold neutron spectroscopy to access the scattering function  $S(Q, \omega)$  depending on the scattering vector  $Q$ , i.e. the reciprocal observation length, and the energy transfer  $\omega$ . The neutron scattering experiment has been carried out on the time-of-flight spectrometer IN6 at the Institut Max von Laue – Paul Langevin (ILL), Grenoble, France, using the incident wavelength  $\lambda = 5.1 \text{ \AA}$ . In this configuration, the weakly  $Q$ -dependent width of the energy resolution function  $R(Q, \omega)$  amounted to approximately  $90 \text{ } \mu\text{eV}$  FWHM. The spider dragline silk sample (Figure 1, top) was obtained from *Nephila edulis* spiders using a forced silking technique [28] and had a total mass of  $m = 104 \text{ mg}$  at ambient humidity. The continuous fiber was wound around a pair of steel hooks and mounted inside the humidity chamber of the tensile machine described in detail in Ref. [17]. The silk sample was oriented such that the axis of the fibers illuminated by the neutron beam was perpendicular to the scattering plane defined by the equatorially mounted detectors. The initial distance between the inner edges of the steal hooks prior to the strain-induced fiber extension amounted to  $30 \text{ mm}$  commensurate with the incident neutron beam height. The humidity chamber holding the sample was placed inside the evacuated sample bay of IN6 and kept at the ambient temperature  $T = 25 \pm 0.5 \text{ K}$ , which was monitored by two Pt100 temperature sensors. The saturated humid ( $\text{H}_2\text{O}$ ) atmosphere inside the chamber was created by small open troughs filled with ultrapure water placed at the bottom of the chamber. The ambient humidity was monitored using two humidity senors and was always saturated within errors during the acquisitions on the humid silk sample. In addition, data on the empty humid chamber, on the sample dried by a vacuum pump, on the empty dry chamber, and on Vanadium metal foil placed in a similar geometry as the fibers were recorded for calibration and background treatment purposes. The spectrum from the dry unstretched spider silk was recorded first during approximately 6 hours. Subsequent to the start of the humidification, spectra were recorded

with a time resolution of 10 minutes to observe and ascertain that a full humidification was obtained, as reflected in the absence of visible changes in the spectra with time and corroborated by the saturated humidity detected by the humidity sensors. When the full humidification was reached, the total recording time per spectrum at each given stress (positions marked by letters in figure 1, bottom, explained further below) amounted to approximately 6 hours. The experiment data are permanently curated by the ILL and accessible by the experiment number 8-04-635.

The data were reduced by applying standard procedures for neutron time-of-flight data using the *lamp* software provided by the ILL and subsequently analyzed using *python*, as described in Ref. [18]. As part of the standard reduction procedures, (i) all intensities were normalized by the incident neutron beam intensity, (ii) the above mentioned separately recorded scattering signal from the empty humid sample chamber was subtracted from the sample scattering signal, and (iii) the quasi-elastic scattering signal was corrected for the so-called overlap background created by neutrons exceeding their initial time frame. The obtained scattering functions  $S(Q, \omega)$  were divided by the self-contained static structure factor, and the thus normalized functions

$$S_n(Q, \omega) = \frac{S(Q, \omega)}{\int_{-\Delta\omega}^{+\Delta\omega} S(Q, \omega) d\omega} \quad (4)$$

with  $\Delta\omega \approx 90\mu\text{eV}$  were used for the analysis of the quasi-elastic scattering. The restricted energy range for the integration in this case also to a good approximation eliminates the effect of the thermal Debye-Waller factor. In contrast, for the diffraction patterns shown in figure 2, the full energy range was taken, corresponding to a diffraction pattern recorded on a diffractometer without energy discrimination. For a comparison of the absolute scattering, the intensities were normalized by the stress-dependent “geometrical” scattering volume of the sample that was illuminated by the neutron beam. This volume was obtained by assuming the conservation of the total sample volume and a constant incident neutron beam cross section.

All experimental spectra  $S(Q, \omega)$  were fitted by the Fourier-transform in time of the model intermediate scattering function  $I(Q, t)$  resulting from the solution of the spatially Fourier-transformed equation 2,

$$I(Q, t) \sim E_{\alpha,1} \left( - \left| \frac{t}{\tau} \right|^\alpha \right) \quad \text{with} \quad \tau = (K_\alpha Q^2)^{1/\alpha}, \quad (5)$$

multiplied with the analytical description of the experimental resolution function  $R(Q, t)$ . In equation 5,  $E_{\alpha,\beta}$  denotes the Mittag-Leffler function already mentioned further above,

$$E_{\alpha,\beta}(z) = \sum_{n=0}^{\infty} \frac{z^n}{\Gamma(\alpha n + \beta)}, \quad (6)$$

and  $\tau$  can be interpreted as the fractional relaxation time. Notably, the fit algorithm is implemented such that  $\alpha$  does not depend in  $Q$ , i.e. the entire experimentally accessed  $Q$ -range is fitted at once by a global fit of the model.

### 3 *In situ* stress-strain curve

The stress-strain curve recorded *in situ* during the neutron scattering experiment on the humid spider silk fibers at 100 % relative ambient humidity from H<sub>2</sub>O is depicted in Figure 1 (bottom). The calibration of the stress  $\sigma$  was based on the assumption of a constant average fiber diameter of 12.5  $\mu\text{m}$  obtained from microscope measurements and a fiber mass density of 1.38 g/cm<sup>3</sup> [29]. It is noted that the fiber diameter depends on the humidity and strain on the fiber. This effect has been neglected for the calculation of the stress  $\sigma$ , because it was impossible to model. For this reason, we will discuss the neutron scattering results in terms of the model-free relative strain  $\epsilon$ .

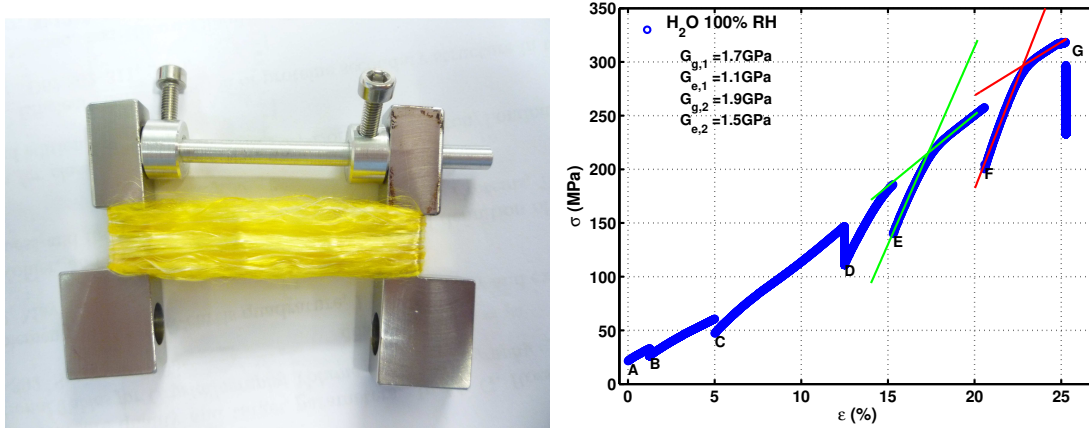


Figure 1: (Color online) Top: Photograph of the spider silk sample used on the neutron time-of-flight spectrometer IN6, depicted along with the steel hooks that were later attached to the tensile machine inside IN6. Bottom: Stress  $\sigma$  versus the externally applied relative strain  $\epsilon$  on the humid spider silk sample recorded *in situ* on IN6. The points marked by capital letters denote the positions where neutron spectra have been recorded. The lines are linear fits used to extract the elastic moduli reported in the legend.

The lines in Figure 1 (bottom) are linear fits to determine the module  $G_g = G + G_e$  of the sample in terms of the three-parameter Maxwell model [8], with  $G_e$  being the elastic and  $G$  the relaxation modulus. The values found here are significantly higher than the corresponding values found for silkworm silk in an earlier experiment by our group [17] which is consistent with the expectation that spider silk is the stronger material.

The capital letters A-G in figure 1 (bottom) mark the positions where the neutron data were recorded. Importantly, due to the long acquisition time of the neutron spectra on the order of a few hours, our neutron scattering experiment observes the long-time asymptotic behavior of the viscoelastic relaxation of the initial stress [8]. This asymptotic relaxation becomes apparent by the dips in the otherwise continuous stress-strain curve (figure 1 (bottom)).

The observed stress-strain curve has to be discussed in the context of the role of water and the stress-dependent capacity of water uptake by the fiber. To this effect, we



note a few observations reported in the literature: When silk filaments are mechanically restrained while being exposed to a high humidity, a tensile force builds up. This force reaches its maximum value within a few minutes after an exposure to 100 % humidity [23, 30]. It appears that some of the adsorbed water is permanently bound [23]. The diameter of major ampullate dragline silk rises from a typical value [31] of  $(2.8 \pm 0.5) \mu\text{m}$  in the dry state to  $(20.4 \pm 6.4) \mu\text{m}$  in the unconstrained fully humid state [31]. When constrained, the diameter of humid silk only reaches a typical value of  $(9.7 \pm 3.5) \mu\text{m}$  [31]. It has therefore been proposed that the water inside the disordered regions of the silk fibers is “pushed out” under tensile load [32]. The mass density of spider silk has been reported as  $1.3 \text{ g/cm}^3$  [33] or  $1.36 \text{ g/cm}^3$  for major ampullate [34]. When fully hydrated, nearly two thirds of the fiber mass is due to water uptake [6], and the volume more than doubles [35]. The hydration water appears to break the hydrogen bonds in the amorphous phase through water bridges at low stress, resulting in a softening of the amorphous chains. Remarkably, it has been hypothesized that, when the stress exceeds a certain threshold assumed to be near 0.2 GPa, the water bridging effect is reversed and the amorphous polymer chains become again stiffer [36]. Our own experimental observations from the *in situ* neutron diffraction pattern, reported in the following section, suggest that our sample took up an increasing amount of water with increasing stress (figure 2, see also the electronic supplementary material).

## 4 *In situ* equatorial diffraction pattern

Within the limits of the large beam divergence on IN6, an approximate in-plane, i.e. equatorial diffraction pattern is obtained by integrating over all time-of-flight channels of the spectrometer IN6 (figure 2, a). Since the scattering is predominantly incoherent and the silk polymer is predominantly amorphous, the diffraction peaks arising from the polyalanine crystallite structure are very weak, although the [110] and [020] peaks are clearly visible (figure 2) and can be tentatively modeled by Gaussian profiles (dashed lines in figure 2, a). For the fitting we assumed an additional third, broader Gaussian (dotted line) as well as a constant background accounting for the prevailing incoherent scattering (horizontal dashed line in figure 2, a). The resulting widths  $\sigma$  of the crystallite peaks appear to change very slightly with the externally applied tensile strain (figure 3). The strain-dependence of the diffraction studied on IN6 can be compared with the pressure dependence as studied by x-rays [37]. This dependence generally agrees with the rearrangement of the crystallites within the fibers, consistent with an alignment along the fiber axis. The intensities in figure 2 have been normalized by the nominal “geometrical” scattering volume that is calculated from the extraction of silk material from the neutron beam with the increasing tensile stress (see the preceding section). Accordingly, the increasing intensities with increasing stress indicate an additional water uptake by the fibers with increasing stress, which counterbalances the forced hindrance of the supercontraction or hydrophobic collapse [22, 25, 26]. For the analysis of the quasi-elastic scattering (section 6) we divide the dynamic scattering function by the static structure

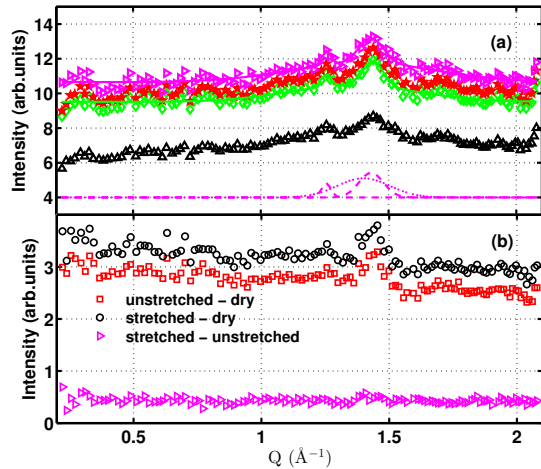


Figure 2: (Color online) (a): Equatorial diffraction patterns (symbols) obtained from the IN6 time-of-flight data by summing all time-of-flight channels (equivalent to a diffraction pattern recorded on a dedicated diffractometer, however, with lower angular resolution). The different symbols, from top to bottom, denote highest stress (magenta  $\triangleright$ -symbols, point G in Fig. 1), medium stress (red  $\star$ -symbols, point C in figure 1) and no stress (green  $\diamond$ -symbols, point A) on humid silk and unstretched dry silk (black  $\Delta$ -symbols), respectively. The solid lines denote fits to polyalanine  $\beta$ -sheet peaks and resulting widths  $\sigma_{020}$  and  $\sigma_{110}$ , represented by one Gaussian function each (dashed lines), plus another broader Gaussian (dotted line), and the constant incoherent background (horizontal dashed line). The intensities have been normalized by the nominal scattering volume (see text). (b): Difference patterns of stretched (point G) and unstretched (point A) with unstretched humid and unstretched dry silk as specified in the legend.

factor to eliminate contributions from this coherent scattering (but in this case restricting the energy integration range, cf. section 2, equation 4). Figure 2 (b) depicts difference patterns explained in the legend. The vanishing peak in the difference of stretched and unstretched humid silk suggests that stress has no significant influence on the peak intensity. The differences between humid and dry silk suggest that the peaks become sharper in the presence of water in the amorphous regions presumably due to a better alignment in the humid silk associated with the better “fluidity”.

## 5 Generalized frequency distribution

Before discussing the diffusive relaxations in the subsequent section, here we briefly address the inelastic scattering from our spider silk sample. These results help to compare spider silk with related other materials such as silkworm silk [7, 17] and elastin [27].

The time-of-flight spectra contain information on the low-energy inelastic scattering up to on the order of 100 meV on the neutron energy gain side of the spectrum, providing access to atomic vibrations. In this region, the water translation and libration modes as



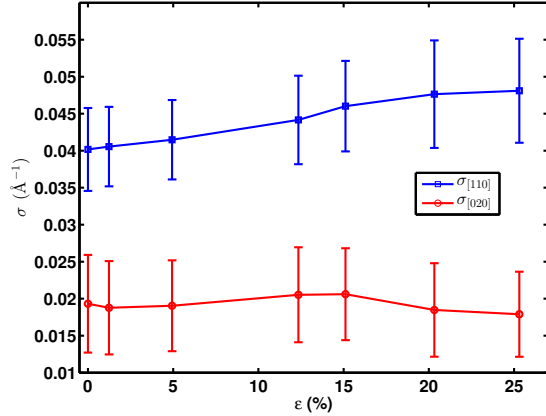


Figure 3: (Color online) Fit results for the widths of the polyaniline  $\beta$ -sheet peaks  $\sigma_{020}$  and  $\sigma_{110}$  (figure 2) as a function of the elongation  $\epsilon$ .

well as some signals from the crystallites of the silk can be observed. For a quantitative analysis, we derive the  $Q$ -integrated generalized frequency distribution  $P(\beta) = \int_{\alpha} P(\alpha, \beta)$  according to [38]

$$P(\alpha, \beta) = 2\beta \sinh(\beta/2) \frac{\tilde{S}(\alpha, \beta)}{\alpha} \quad (7)$$

from the scattering function  $\tilde{S}$  in the reduced coordinates

$$\alpha = \frac{\hbar^2 Q^2}{2Mk_B T} \quad \text{and} \quad \beta = \frac{\hbar^2 \omega}{k_B T} \quad (8)$$

with the atom mass  $M$ .

The generalized frequency distribution (figure 4) reveals the water libration peak maximum in humid spider silk near  $(-66 \pm 0.01)$  meV, which is similar to the libration peak position found for humid silkworm silk [17]. The shift with strain of the librational peak for spider silk is not significant within the statistical errors. The librational peak intensity appears to change with stretching, but we note that the peak intensities may also be affected by a possibly underlying slow process of permanent binding of water associated with the supercontraction [23].

The low-frequency water librations are sensitive to localized hydrogen bonding and steric restrictions [39]. The higher the position of the libration peak is in absolute energy values, the stronger the adsorbed water is geometrically confined [40]. Another peak can be observed near  $-30$  meV. A similar peak found for silkworm silk at  $-28$  meV has been tentatively assigned to a vibrational mode of the crystallites [7]. As for silkworm silk, this peak vanishes in the difference spectra humid - dry in agreement with the assumption that this peak arises from the crystallites which are not accessible to water [7]. Besides the crystalline peak, the region between  $-20$  and  $-30$  meV is dominated by hydrogen translations [39].

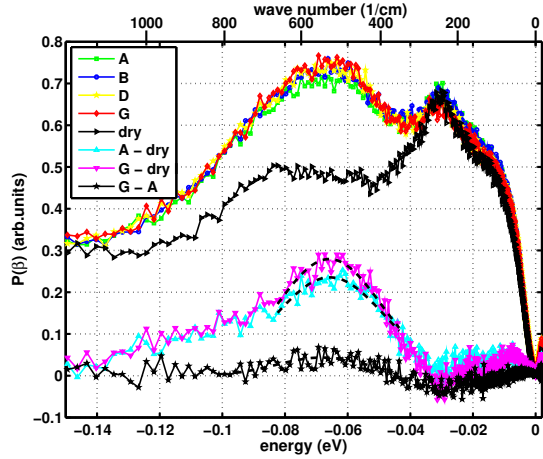


Figure 4: (Color online)  $Q$ -integrated generalized frequency distribution calculated from the time-of-flight spectra on the spider silk sample in the dry and humid (100% RH  $H_2O$ ) state, respectively, for different strains. The letters “A” to “G” refer to the humid spider silk sample at the different strains where neutron spectra were recorded, as shown in figure 1 (bottom). The dashed lines superimposed on the difference spectra “A - dry” and “G - dry”, respectively, are indicative fits of a Gaussian line shape to determine the position of the maximum of the water librational peak.

## 6 Quasi-elastic neutron scattering

The essential information for the present study is contained in the so-called quasi-elastic scattering (QENS) recorded on the neutron time-of-flight spectrometer, i.e. the apparent broadening of the instrumental resolution. This QENS signal carries the information from the picosecond diffusive or relaxation motions and in our study is subject to the modeling based on the fractional diffusion. Figure 5 depicts example spectra (symbols) at a fixed scattering vector  $Q$  for different values of the externally applied strain  $\epsilon$ . The plot first of all illustrates the model-free observation of an increasing broadening of the spectra with increasing strain. This observation of a faster diffusive molecular mobility with increasing tensile strain is consistent with the hypothesis of strain-softening in partially glassy polymeric nanocomposite materials [41], and the same trend has been found for humid silkworm silk [17]. The superimposed lines in figure 5 denote the fits with the model of fractional Brownian diffusion as will be explained along with the subsequent figure. Figure 6 depicts spectra (symbols) for several values of the scattering vector  $Q$  recorded on stretched humid spider silk at a fixed strain  $\epsilon$  and fits with the model of fractional diffusion, i.e. with the numerically performed time Fourier transform of equation 5 (lines). The fractional model accurately describes the spectra in this simultaneous fit with global values for  $\alpha$  and  $K_\alpha$  that apply for all recorded scattering vectors  $Q$ . This shows that the observed  $Q$ -dependent spectral linewidths  $\Gamma(Q)$  follow a generalized Brownian diffusion  $\Gamma(Q) = K_\alpha Q^2$  with a generalized  $Q$ -independent diffusion coefficient  $K_\alpha$ .

Figure 7 summarizes the obtained fit parameters of equation 5, namely  $\alpha$  and  $K_\alpha$  as

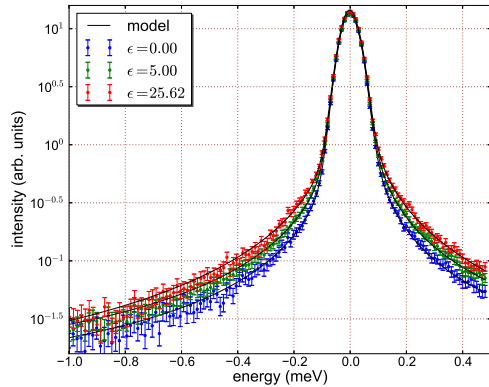


Figure 5: (Color online) QENS spectra for different values of the stress applied to the hydrated fibers (points A, C, G in figure 1) at a fixed value of the scattering vector  $Q = 1 \text{ \AA}^{-1}$  (symbols) and fit with the fractional model (lines). The figure illustrates the model-free observation of an increasing broadening of the QENS spectra from the humid spider silk fibers with increasing externally applied stress.

well as the generalized relaxation time or reciprocal spectral linewidth  $\tau(Q) = 1/\Gamma(Q)$  as a function of the applied tensile strain. Within the experimental accuracy, we observe the trend of a monotonous dependence of all three parameters on the tensile strain. Both the memory parameter  $\alpha$  as well as the diffusion coefficient  $K_\alpha$  increase with the applied stress. The increase of  $K_\alpha$  is consistent with the generally faster molecular mobility in the amorphous fraction of the spider silk that was also observed on a smaller data set for silkworm silk [17, 18].  $K_\alpha$  rises strongly with the first strain step, and the functional dependence  $K_\alpha(\epsilon)$  appears to follow an asymptotic behavior. The strong increase of  $K_\alpha$  with the first strain step corresponds to the transition from the native (stable) to the pre-stretched (meta-stable) viscoelastic state of the fiber [8]. The increase of  $\alpha$  is consistent with an increasing loss of memory or entropy with rising stress, in agreement with the picture of entropy elasticity [35]. ( $\alpha = 1$  would correspond to simple Brownian diffusion.) Finally, the decrease of  $\tau$  (shown for one example  $Q$ -value in figure 7) illustrates the increase of the spectral linewidth with rising stress. The latter result is consistent with the aforementioned model-free observation of the increasing broadening of the spectral width  $\Gamma(Q) = 1/\tau(Q)$  with rising stress that can be observed by just superimposing the spectra and not applying any fit (cf. figure 5).

We tentatively associate the observed mobility with the water-accessible disordered regions [14] of the fibers, because results on the morphologically similar silkworm silk fibers suggest that the crystalline  $\beta$ -sheets do not contribute to the diffusive mobility on our observation scale [7]. Nevertheless, our model is independent from the state of the material and describes statistically correlated cooperative molecular dynamics independently from the location of the dynamics inside the material. A strong cooperation effect of molecules in the disordered amorphous matrix, water molecules, and perhaps  $\beta$ -sheet molecules may

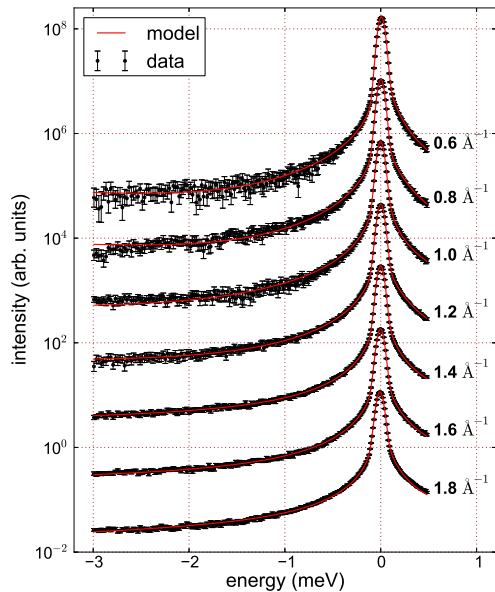


Figure 6: (Color online) QENS spectra at point D in figure 1 for different values of the scattering vector  $Q$  (symbols) and fit with the fractional model (lines). All  $Q$ -values were fitted at once by the Fourier transform of equation 5 multiplied with the experimental resolution.

be at the origin of the fractionality of the observed dynamics.

## 7 Conclusions

Hydrated spider dragline silk fibers allow us to measure and model the ensemble-averaged self-diffusive mobility of the hydrogen atoms in the amorphous polymer fraction on picosecond time and nanometer length scales using incoherent neutron spectroscopy. This diffusion is associated with the mobility of both the absorbed water and the polymer chains themselves and can be consistently described by a generalized fractional diffusion coefficient  $K_\alpha$  which does not depend on the scattering vector  $Q$ , i.e. the reciprocal observation length scale, in the observed nanometer range. We find a monotonously increasing dependence of  $K_\alpha$  and  $\alpha$  on the externally applied tensile strain. This observation is consistent with a faster diffusion (rising  $K_\alpha$ ) and increasing order and synonymously decrease of the entropy or memory within the initially rather randomly arranged polymers (rising  $\alpha$ ). The absolute values for  $\alpha$  are smaller for spider silk than for silkworm silk, which is consistent with a higher degree of disorder in spider silk. The absolute values for  $K_\alpha$  are also smaller by this comparison in agreement with an overall slower diffusivity in spider silk compared to silkworm silk. Moreover, the fractional relaxation times in spider silk are significantly larger than those found for silkworm silk at similar strain. All of these

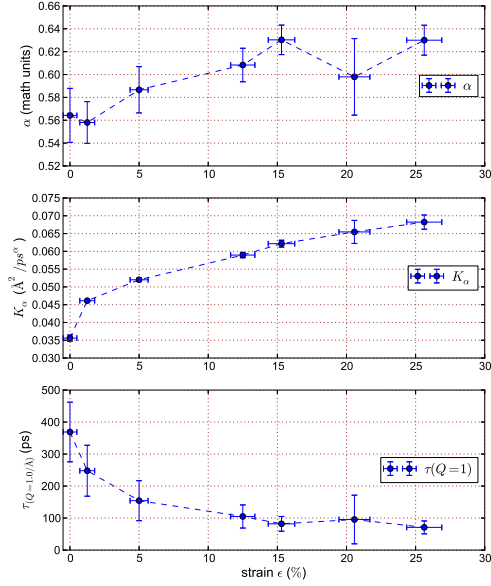


Figure 7: (Color online) Summary of the fit results (symbols) for the parameters of the fractional model, equation 5, namely the memory parameter  $\alpha$ , the generalized diffusion coefficient  $K_\alpha$ , and the relaxation time  $\tau = (K_\alpha Q^2)^{1/\alpha}$  (taken at  $Q = 1 \text{ \AA}^{-1}$ ), for the different strains on the spider silk fibers as marked in figure 1 (A-G). The dashed lines are guides to the eye.

differences between spider silk and silkworm silk corroborate the assumption that a higher degree of “fractionality”, i.e. stronger memory effects on the molecular level, enhances the macroscopic mechanical properties. Considering that spider silk is a highly complex material that undergoes substantial structural rearrangements upon mechanical load and uptake of water, it is remarkable that the molecular mobility can be fully described by a model that contains only very few parameters. Moreover, these resulting parameters display a simple asymptotic functional dependence on the tensile strain. Our results may contribute to establishing a link between the molecular mobility and macroscopic mechanical properties, and to a general understanding of polymer nanocomposite materials for instance in the context of models of strain softening.

## Data accessibility

The neutron data are permanently curated by the ILL under the experiment number 8-04-635 (cycle 114, run numbers 150907 to 151295) and freely accessible via <http://barns.ill.eu>.

## Electronic supplementary material

Electronic supplementary material is available.

## Competing interests

We have no competing interests.

## Authors' contributions

All authors designed and coordinated the research and contributed to drafting the manuscript. IG and FV provided the spider silk sample. TS, IG, MB, and MM carried out the neutron scattering experiment. TS reduced the data and analysed the stress-strain curve, diffraction patterns and vibrational spectra. IK implemented and performed the fits of the fractional model. All authors gave final approval for publication.

## Acknowledgement

We are grateful to M. Koza (ILL) for advice and help regarding the spectrometer IN6. We thank W. Press and W. Knoll (both U Kiel) for stimulating discussions, and R. Ammer and S. Jenkins (both ILL) for technical support at IN6, and the ILL for the allocation of neutron beam time. The tensile machine and its humidity chamber have been constructed by the machine shop team at the IEAP, University of Kiel.

## Funding

This work was in part supported by the Deutsche Forschungsgemeinschaft (DFG) SFB 677 “Function by switching”, and FV was supported by the AFSOR.

## References

- [1] Gersappe D. Molecular mechanisms of failure in polymer nanocomposites. *Physical Review Letters*. 2002;89(5):058301.
- [2] Porter D, Guan J, Vollrath F. Spider silk: super material or thin fibre? *Advanced Materials*. 2013;25(9):1275–1279.
- [3] Shah DU, Porter D, Vollrath F. Can silk become an effective reinforcing fibre? A property comparison with flax and glass reinforced composites. *Composites Science and Technology*. 2014;101:173–183.



- [4] Gosline JM, DeMont ME, Denny MW. The structure and properties of spider silk. *Endeavour*. 1986;10(1):37–43.
- [5] Vollrath F, Porter D. Spider silk as archetypal protein elastomer. *Soft Matter*. 2006;2(5):377–385.
- [6] Vehoff T, Glisovic A, Schollmeyer H, Zippelius A, Salditt T. Mechanical Properties of Spider Dragline Silk: Humidity, Hysteresis, and Relaxation. *Biophysical Journal*. 2007;93(12):4425 – 4432.
- [7] Seydel T, Kölln K, Krasnov I, Diddens I, Hauptmann N, Helms G, et al. Silkworm silk under tensile strain investigated by synchrotron x-ray diraction and neutron spectroscopy. *Macromolecules*. 2007;40:1035–1042.
- [8] Krasnov I, Diddens I, Hauptmann N, Helms G, Ogurreck M, Seydel T, et al. Mechanical properties of silk: Interplay of deformation on macroscopic and molecular length scales. *Physical Review Letters*. 2008;100(4):048104.
- [9] de Tommasi D, Puglisi G, Saccomandi G. Multiscale mechanics of macromolecular materials with unfolding domains. *Journal of the Mechanics and Physics of Solids*. 2015;78:154–172.
- [10] Nova A, Keten S, Pugno NM, Redaelli A, Buehler MJ. Molecular and Nanostructural Mechanisms of Deformation, Strength and Toughness of Spider Silk Fibrils. *Nano Letters*. 2010;10(7):2626–2634.
- [11] Termonia Y. Molecular Modeling of Spider Silk Elasticity. *Macromolecules*. 1994;27(25):7378–7381.
- [12] Vollrath F, Knight DP. Liquid crystalline spinning of spider silk. *Nature*. 2001;410(6828):541–548.
- [13] Riekel C, Gutierrez MCG, Gourrier A, Roth S. Recent synchrotron radiation microdiffraction experiments on polymer and biopolymer fibers. *Analytical and Bioanalytical Chemistry*. 2003;376(5):594–601.
- [14] Sapede D, Seydel T, Forsyth VT, Koza MM, Schweins R, Vollrath F, et al. Nanofibrillar structure and molecular mobility in spider dragline silk. *Macromolecules*. 2005;38(20):8447–8453.
- [15] Hakimi O, Knight DP, Knight MM, Grahn MF, Vadgama P. Ultrastructure of insect and spider cocoon silks. *Biomacromolecules*. 2006;7(10):2901–2908.
- [16] Keten S, Buehler MJ. Nanostructure and molecular mechanics of spider dragline silk protein assemblies. *Journal of The Royal Society Interface*. 2010;7(53):1709–1721.

- [17] Seydel T, Knoll W, Greving I, Dicko C, Koza MM, Krasnov I, et al. Increased molecular mobility in humid silk fibers under tensile stress. *Physical Review E*. 2011;83:016104.
- [18] Krasnov I, Seydel T, Müller M. Fractional dynamics in silk: From molecular picosecond subdiffusion to macroscopic long-time relaxation. *Physical Review E*. 2015;91(4):042716.
- [19] Metzler R, Klafter J. The random walk’s guide to anomalous diffusion: a fractional dynamics approach. *Physics reports*. 2000;339(1):1–77.
- [20] Heymans N, Bauwens JC. Fractal rheological models and fractional differential equations for viscoelastic behavior. *Rheologica Acta*. 1994;33(3):210–219.
- [21] Van Beek JD, Beaulieu L, Schäfer H, Demura M, Asakura T, Meier BH. Solid-state NMR determination of the secondary structure of *Samia cynthia ricini* silk. *Nature*. 2000;405(6790):1077–1079.
- [22] Work RW. A comparative study of the super-contraction of major ampullate silk fibers of orb-web-building spiders (araneae). *Journal of Arachnology*. 1981;9(3):299–308.
- [23] Agnarsson I, Boutry C, Wong SC, Baji A, Dhinojwala A, Sensenig AT, et al. Supercontraction forces in spider dragline silk depend on hydration rate. *Zoology*. 2009;112(5):325–331.
- [24] Blackledge TA, Boutry C, Wong SC, Baji A, Dhinojwala A, Sahni V, et al. How super is supercontraction? Persistent versus cyclic responses to humidity in spider dragline silk. *Journal of Experimental Biology*. 2009;212:1981–1989.
- [25] Cheung MS, García AE, Onuchic JN. Protein folding mediated by solvation: Water expulsion and formation of the hydrophobic core occur after the structural collapse. *Proceedings of the National Academy of Sciences*. 2002;99(2):685–690.
- [26] Zhou R, Huang X, Margulis CJ, Berne BJ. Hydrophobic collapse in multidomain protein folding. *Science*. 2004;305(5690):1605–1609.
- [27] Perticaroli S, Ehlers G, Jalarvo N, Katsaras J, Nickels JD. Elasticity and Inverse Temperature Transition in Elastin. *The Journal of Physical Chemistry Letters*. 2015;6(20):4018–4025.
- [28] Work RW, Emerson PD. An apparatus and technique for the forcible silking of spiders. *Journal of Arachnology*. 1982;10:1–10.
- [29] Zhao HP, Feng XQ, Shi HJ. Variability in mechanical properties of *Bombyx mori* silk. *Materials Science and Engineering: C*. 2007;27(4):675 – 683.

- [30] Guinea GV, Elices M, Perez-Rigueiro J, Plaza G. Self-tightening of spider silk fibers induced by moisture. *Polymer*. 2003;44(19):5785–5788.
- [31] Work RW. Dimensions, birefringences, and force-elongation behavior of major and minor ampullate silk fibers from orb-web-spinning spiders: The effects of wetting on these properties. *Textile Research Journal*. 1977;47(10):650–662.
- [32] Brown CP, MacLeod J, Amenitsch H, Cacho-Nerin F, Gill HS, Price AJ, et al. The critical role of water in spider silk and its consequence for protein mechanics. *Nanoscale*. 2011;3(9):3805–3811.
- [33] Agnarsson I, Dhinojwala A, Sahni V, Blackledge TA. Spider silk as a novel high performance biomimetic muscle driven by humidity. *Journal of Experimental Biology*. 2009;212(13):1990–1994.
- [34] Stauffer SL, Coguill SL, Lewis RV. Spider silk as a novel high performance biomimetic muscle driven by humidity. *The Journal of Arachnology*. 1994;22(1):5–11.
- [35] Gosline JM, Denny MW, Demont ME. Spider silk as rubber. *Nature*. 1984;309(5968):551–552.
- [36] Ene R, Papadopoulos P, Kremer F. Combined structural model of spider dragline silk. *Soft Matter*. 2009;5:4568–4574.
- [37] Ene R, Krywka C, Kang SG, Papadopoulos P, Burghammer M, Cola ED, et al. Structure changes in Nephila dragline: The influence of pressure. *Polymer*. 2012;53:5507–5512.
- [38] Fontana A, Rocca F, Fontana MP, Rosi B, Dianoux AJ. Low-frequency dynamics in superionic borate glasses by coupled Raman and inelastic neutron scattering. *Physical Review B*. 1990;41(6):3778–3785.
- [39] Ockwig NW, Cygan RT, Hartl MA, Daemen LL, Nenoff TM. Incoherent inelastic neutron scattering studies of nanoconfined water in clinoptilolite and heulandite zeolites. *Journal of Physical Chemistry C*. 2008;112(35):13629–13634.
- [40] Crupi V, Majolino D, Migliardo P, Venuti V. Diffusive relaxations and vibrational properties of water and H-bonded systems in confined state by neutrons and light scattering: State of the art. *Journal of Physical Chemistry A*. 2000;104(47):11000–11012.
- [41] Allegra G, Raos G, Vacatello M. Theories and simulations of polymer-based nanocomposites: from chain statistics to reinforcement. *Progress in Polymer Science*. 2008;33(7):683–731.